Proceedings of CHT-08
ICHMT International Symposium on Advances in Computational Heat Transfer

May 11-16, 2008, Marrakech, Morocco

CHT-08-249

TURBULENT FORCED CONVECTION IN A HORIZONTAL CHANNEL WITH RECTANGULAR OBSTACLE

Annabelle Joulin[*,§], Yassine Cherif[*], Laurent Zalewski[*] Stéphane Lassue, and Daniel Rousse[⌘]
[*]LAMTI, Faculté des Sciences Appliquées de l'université d'Artois, Béthune, France
[⌘]Department of applied sciences, Université du Québec à Chicoutimi, Canada
[§]Correspondence author. Fax: +33 321 632 356 Email: annabelle.joulin@univ-artois.fr

ABSTRACT This paper presents a numerical investigation of turbulent forced convective flow in a horizontal channel filled with rectangular obstacles located on the lower surface. An exchanger isothermal test plate is embedded in the lower wall, in the fully developed region of the flow. Immediately above this plate, on the upper surface, a black coated isothermally heating resistance facing downwards is installed. This perfectly absorbing surface provides a controlled radiative heat flux on the lower test plate. In this study, custom-built tangential gradient fluxmeters (TGFM) are used to provide local measurements of convective heat transfer so as to validate the numerical predictions. Then, parametric studies are carried out. The profiles for the heat flux densities are presented for different Reynolds numbers in the flow direction along the cold isothermal lower plate. The influence of the presence of an obstacle on the heat flux densities is also investigated. All numerical predictions are carried out with Fluent, previously calibrated against benchmark problems and experimental measurements. In the paper, special emphasis is given in the systematic comparison between experimental and numerical results.

INTRODUCTION

The way and rate at which heat is transferred is investigated for numerous domestic, transportation, commercial, and industrial applications. Specific applications related to this study namely involve cooling of electronic components, building air conditioning, compact heat exchanger, and efficient heat recovery from low temperature sources. For most of these applications, the accurate knowledge of heat exchanges between a surface that may involve several protuberances and its surrounding is essential to ensure an efficient or optimized system in terms of energy consumption and pollutants production.

In this context, one of the thermal analyst problems is often to ascertain coherent values for the heat transfer coefficient to be use in the simple Newton's law of heat transfer. Several methods have been used over the past century to obtain correlations providing appropriate values of the heat transfer coefficient denoted *h* (Bejan, [1995], Burmeister [1993]). This coefficient is sometimes obtained by use of simplifying approaches consisting of transfer linearization summarized in the standard textbooks by Holman, [2002] and Incropera *et al.*, [2006]. In general, to delineate it, one necessarily has to rely on temperature and/or heat flux measurements. Even though temperature measurement is relatively easy, thermal flux determination is being no means an easy task. As a result, experimental methods are generally based on temperature measurements. The main problem arises from the assumption that the heat transfer coefficient is a constant, whereas the system is thermally unsteady to allow detecting temperature variations (Tsirel, [1973], Sternfield, [1977], Wong, [1979]). We thus consider that it hardly varies. Whether heat flux sensors exist, their principles are mostly based on the use of a seam of thermocouples (Kobus, [2005], Degenne,

[1985]). Using this approach for heat flux determination calls for a rigorous uncertainty analysis as the thickness of the probes (several mm) and their influence (distortion) on measurements can not be neglected. Finally, another method used to determine heat transfer coefficients is to carry out numerical predictions of heat rates.

The first objective of this study aims at determining the spatial heat flux distribution in the flow direction, with and without obstacles, in manner to enable the analyst to propose suitable values of the heat transfer coefficient for several configurations of a tunnel involving obstacles. The research involves two methodological approaches: 3D numerical simulations and parametric studies benchmarked with selected experimental measurements of heat fluxes and temperature.

The numerical investigations were carried out with Fluent, which was first tested against selected force convection flows for which comparable solutions are available in the literature. Then, Fluent predictions were directly confronted to measurements for specific steady-state conditions.
To benchmark the predictions, a rectangular heated wind tunnel is installed in a controlled isothermal room in order to avoid external heat gains or losses. The fluxmeters used in this work are custom-built and designed by the LAMTI researchers Leclercq and Thery [1983]. They are called tangent gradient flux meters (TGFM) because their internal structure generates very small temperatures gradients (on thermoelectric junctions - Copper/Constantan) in the plane of the sensor. This enables the analyst to use a sensor of reduced thickness (a few tenth of mm) therefore lowering the distortion on the measurements (ASTM, [1985]). In this study, TGFM (Lassue, [1989]) are used to measure local convective heat transfer while temperatures are obtained with micro-scale thermocouples (of ~0,1 mm diameter) and local velocities are measured by use of hot wire anemometers (Lefebvre, [1986]).

PHYSICAL PROBLEM AND EXPERIMENTAL SETUP

The rectangular heated wind tunnel used in this study is schematically depicted in Figure 1. This tunnel is located in an isothermal environment in order to prevent any heat transfer from external disturbances. The velocity at the channel's inlet (left in Fig,1) is made uniform by means of a

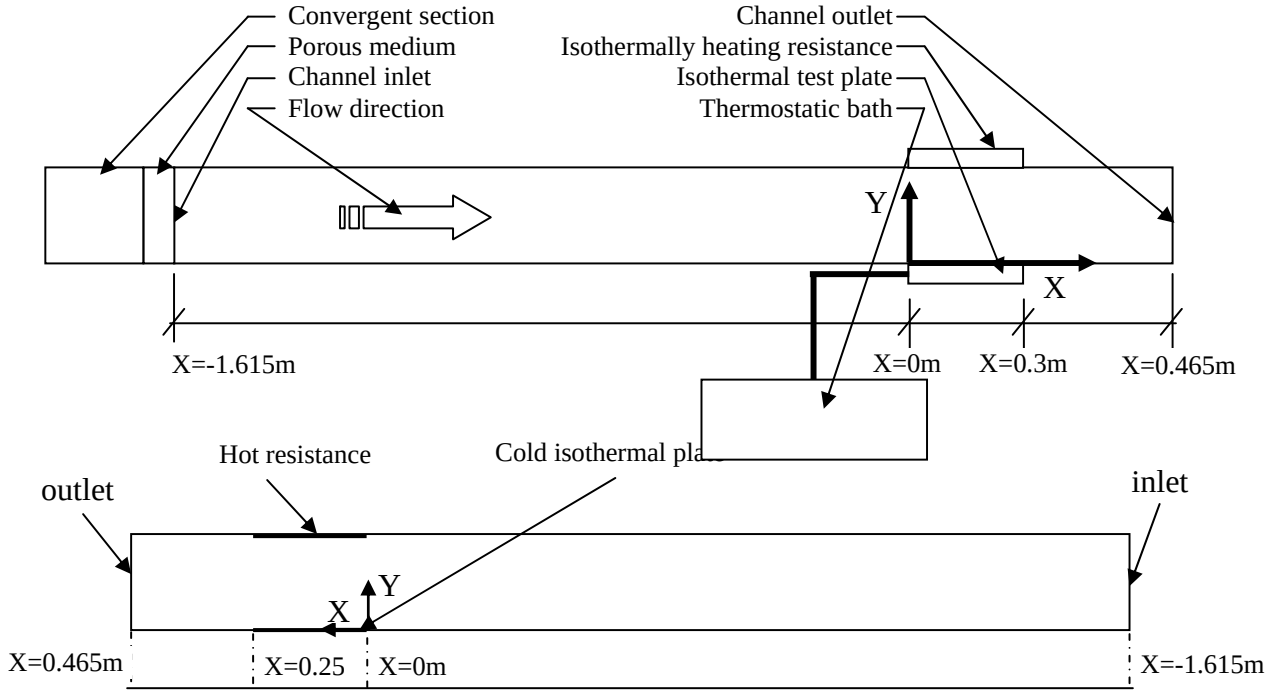

Figure 1a: Geometry of the channel (2D projection)

convergent section and a layer of porous medium installed behind a perforated wire netting. The channel testing length is 2,08 m, the rectangular cross-section is (0,37x0,08 m^2), and the air velocity can vary between 0 and 8 m/s.

A heat exchanging plate (25x30 cm^2) is fitted in the lower wall at 1,615 m downstream of the channel inlet in order to set it in a fully developed flow. This plate is an isothermal wall by means of a thermostatic bath regulating temperature to within 0,1°C. To determine the heat flux densities in this channel, ten TGFMs of dimensions (15 cm long and 1 cm wide) and uniformly spaced 1 cm apart, are inserted rigorously flush in the lower plate to avoid flow disturbances (Figure 1b). To ensure a uniform temperature over the whole plate, a thin copper plate is glued on the top of the heat exchanger plate, creating a thin 1 mm plate's thickness. This plate is covered with a coat of black matte paint, absorbing thermal flux radiation by an upper isothermally heating resistance, of (30x30 cm^2) section, facing downwards. This configuration provides radiation between both plates as well as forced convection. The temperature of the upper hot plate is maintained isothermal and the temperature of the lower cold plate is controlled by a computer and a PID regulator. Twelve thermocouples of T-type pre-calibrated at 0,1K, judiciously located at various sites in the channel, evaluate the wall and air temperatures. The fluxmeters are calibrated at 3%.

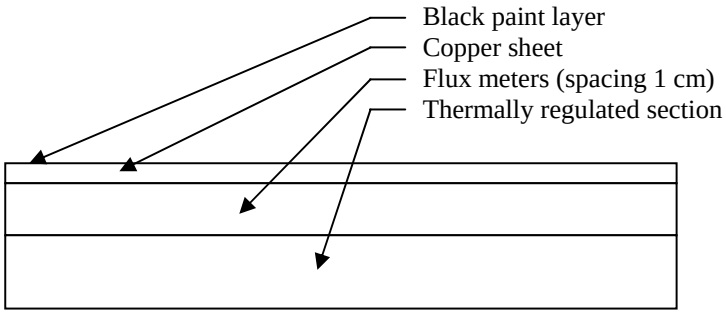

Figure 1b: Detail of the isothermal lower wall involving the flux meters

NUMERICAL METHOD AND SELECTED DETAILS

All numerical simulations are carried out with Fluent. The above described apparatus is discretized using the built-in modeller Gambit (within Fluent) which provides the appropriate non-uniform Cartesian grids for the study. The model is designed to allow specific boundary conditions on each surface. The flow is prescribed to be steady, turbulent, and incompressible. The thermo-physical properties are all assumed to be constant.

The set of governing equations can be found in the Fluent guide (Fluent, [2003]) and will not be repeated here as they are well known to the heat transfer community. The governing parameters which appear in this problem are the Reynolds number based on the hydraulic diameter (D_h=0,13 m) of the channel $Re = U_0 \frac{D_h}{v}$ and the Prandtl number (here 0.71).

The radiative transfer equation is solved using the discrete ordinates (DO) model for a finite number of discrete finite angles (angular discretization S4), each associated with a vector direction.

The fluid is assumed to enter the channel at ambient temperature T_0 and at constant velocity U_0. All the channel (isothermal) walls are assumed to be at the constant ambient air temperature T_0, except for the two parts of the domain where the emitting and absorbing plates are located. On these plates, temperature is set to T_1 and T_2. At the downstream boundary, the pressure is assumed to be equal to the ambient pressure.

The governing equations are discretized following a standard finite volume procedure and the SIMPLE algorithm (Patankar, [1980]) is employed for the velocity-pressure coupling. The momentum, the turbulence kinetic energy, the turbulence dissipation rate, and the energy equations are discretized using a second order upwind scheme. Under-relaxation coefficients were found to be required to control the advancement of the solution field without spurious and undesirable oscillations. A grid refinement around the zone of measurement was proposed to determine the adequacy of the mesh scheme and to ensure that the solutions are grid independent.

Four grid sizes were evaluated as shown in Figure 2, and have been tested to ensure the results are grid independent. In Figure 2, heat fluxes are plotted versus the flow direction over the ten fluxmeters for Re=10400. The non uniform grids involve respectively 66600, 124714, and 164714 control volumes.

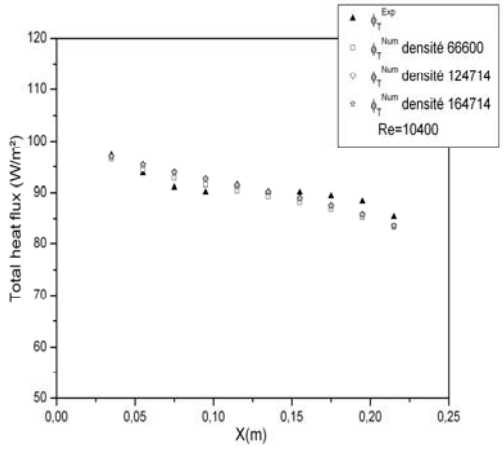

Figure 2: Grid sensitivity test, Re=10400, T_0=295.7K, cold isothermal plate T_1=291.6K and hot resistance temperature T_2=303.5K

As shown in Figure 2, increasing the grid size above 124714 elements does not significantly changes the heat flux prediction over the plate for Re = 10400. Several other tests were carried out for variable Reynolds number with similar results.

Note that the relative discrepancy between the experimental and the numerical results lies between 1% and 4%.
Standard wall functions have been used throughout the test procedure. These acknowledged functions have been successfully used in numerous industrial applications (Launder and Spalding, [1974]). For a convenient simulation, Fluent requires to set some prescribed conditions; the Y^+ value has to be set between 30 and 300 (Fluent, [2003]), with:

$$Y^+ = \frac{Y_P . U_\tau}{\nu} ,$$

where U_τ is the friction velocity, and Y_P is the distance to the wall. Y^+ is a mesh dependent dimensionless length that quantifies to what degree the wall layer is resolved. For a turbulent flow, Y^+ has to be set to more than 30. This condition is verified in order to analyze two different turbulence models, the k-ε model with a standard wall function and the RNG k-ε with a standard wall function. Figure 3 presents the Y^+ values over the ten fluxmeters for three Reynolds numbers. It can be observed that the Y^+ values range between 29 and 75. This permits the use of a turbulence model with a standard wall function and furthermore it enables to obtain numerical results at relatively low computational cost.

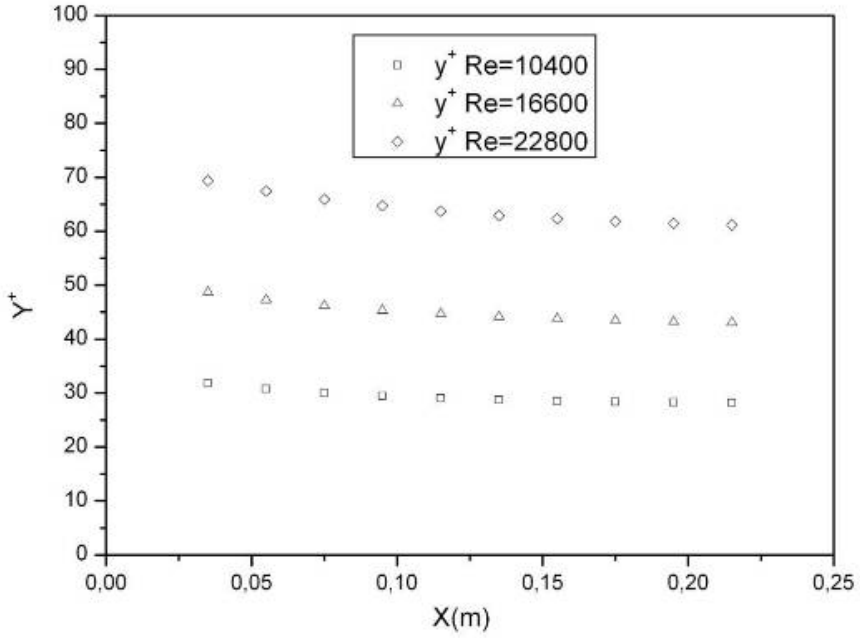

Figure 3. Y^+ values in the flow direction for Re=10400, 16600, and 22800.

After this test pertaining to the appropriateness of the use of a standard wall function, the three dimensional numerical simulations were compared with experimental results in attempts to select the most suitable turbulence model to simulate the flow and the heat transfer in this channel. The RNG k-ε model and the k-ε model are hence used with wall treatment.

Figure 4 presents the results for three different values of Reynolds number and small temperature differences. Air temperature T_0=295.7 K, cold isothermal plate T_1=291.6K and hot resistance temperature T_2=303.5K

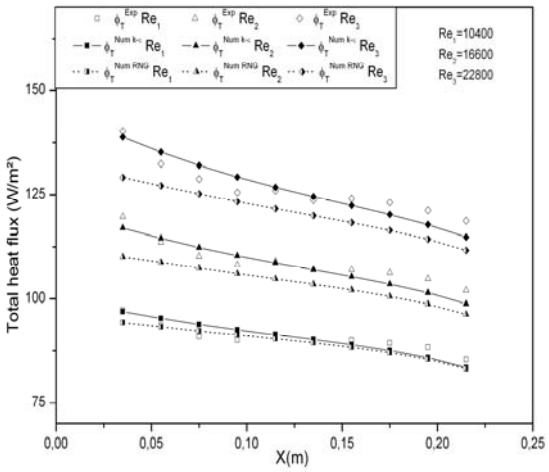

Figure 4. Comparison of the total heat flux densities between the k-ε model and the RNG k-ε model for three different Reynolds numbers Re_1=10400, Re_2=16600 and Re_3=22800. Air temperature T_0=295.7 K, cold isothermal plate T_1=291.6K and hot resistance temperature T_2=303.5K

Figure 4 represents the spatial evolution of the heat flux in the flow direction. The comparison of the results provided by the two models of turbulence reveals a coherent numerical prediction with measurements. On the quantitative level, the RNG *k*-ε prediction curves are always below the standard *k*-ε curves which provide predictions closer to the experimental measurements. The

maximal relative discrepancy with experimental data is not higher than 5%. Therefore, although the *k*-ε and RNG *k*-ε models provide realistic predictions of the heat flux densities, in the following section, all the results are presented for the *k*-ε model which is found better here.

RESULTS

Part 1: Spatial evolution of total heat flux in the flow direction Figure 5 shows the total heat flux measured by each flux meter and represents its spatial behaviour for several flow velocities. As in the previous experiment, the heat flux value is averaged over the sensor's whole surface (15cmx1cm). Figure 5 indicates a monotonic decrease in the total flux in the flow direction at constant temperature and velocity due to an increase of the thickness of the thermal boundary layer. With a constant temperature difference between the two plates, that is, for a constant impinging radiative flux), the total heat flux increases with velocity. As the next figures will clearly indicate, the convective component of the total heat flux is that which governs the evolution.

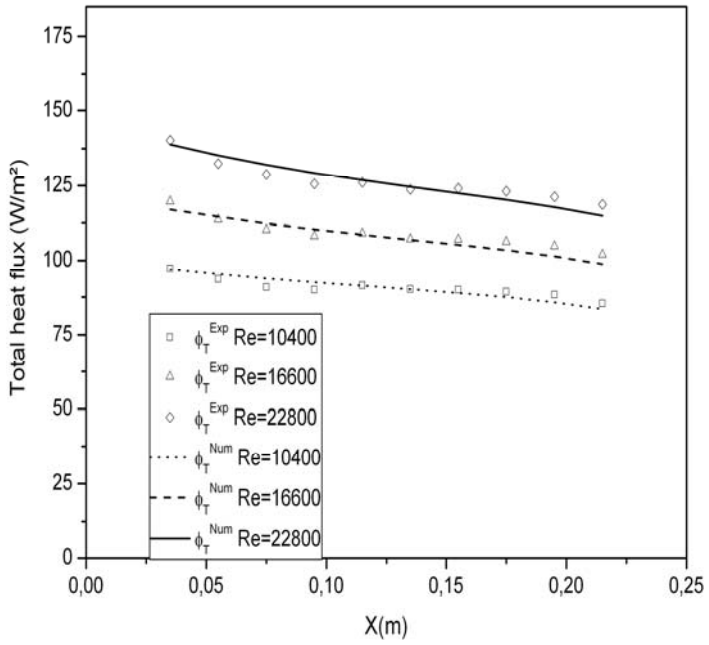

Figure 5. Total heat flux density in the flow direction for different Reynolds numbers Re=10400 (dotted line), Re=16600 (dashed line) and Re=22800 (solid line), symbols represent experimental values. Air temperature is T_0 =295.7 K, cold isothermal plate T_1=291.6K and hot resistance temperature T_2=303.5K

The convective heat flux variation with respect to the X-axis is presented in figure 6, while the radiative heat flux variations are the subject matter of the results presented in figure 7.

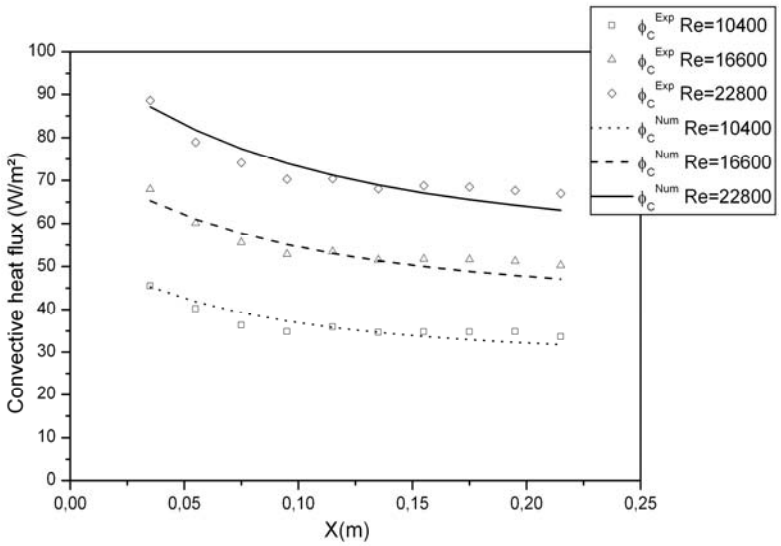

Figure 6. Convective heat flux density in the flow direction for different Reynolds numbers Re=10400 (dotted line), Re=16600 (dashed line) and Re=22800 (solid line), symbols represent experimental values. Air temperature is T_0 =295.7 K, cold isothermal plate T_1=291.6K and hot resistance temperature T_2=303.5K

Consequently, there is a direct consequence over the ration of the radiative flux to the total flux. Figure 7 indeed shows that the radiative flux is independent of the flow velocity and symmetric with respect to the centre of the lower plate. Here, the ratio of the radiative flux to the total flux varies between 48 (W/m^2) on the edges and 52 (W/m^2) in the centre of the plate.

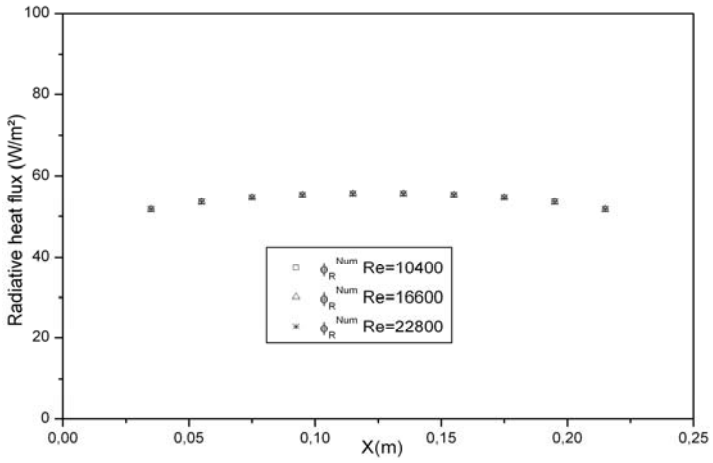

Figure 7. Radiative heat flux density in the flow direction for different Reynolds numbers Re=10400 (dotted line), Re=16600 (dashed line) and Re=22800 (solid line), symbols represent numerical values. Air temperature is T_0 =295.7 K, cold isothermal plate T_1=291.6K and hot resistance temperature T_2=303.5K

Another series of experiment was carried out to observe the evolution of the total flux versus temperature at constant velocity (figure 8). One can notice on figure 8 that heat flux increases with increasing upper plate temperature.

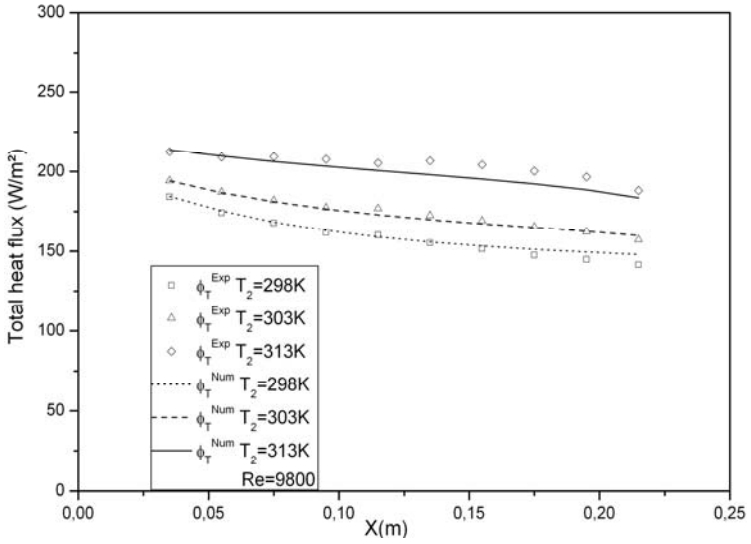

Figure 8. Total heat flux density in the flow direction for different temperature gradients ΔT_1=26 K with T_2=313K (solid line), ΔT_2=16 K with T_2=303K (dashed line) and ΔT_3=11 K with T_2=298K (dotted line). Reynolds number is constant Re = 9800 and air temperature is T_0 =297 K, symbols represent experimental values.

Another check is carried out to ensure the validity of the proposed predictions. Both the numerical and the experimental results were compared to the acknowledged Colburn's correlation (figure 9). Figure 9 shows the experimental and numerical local Nusselt number Nu_x for three different values of the Reynolds number. Results indicate that the solutions proposed herein are in good agreement with those reported by Bejan (1995) who presented the Colburn correlation.

$$Nu_x=0.0296*Re_x^{4/5}*Pr^{1/3}$$

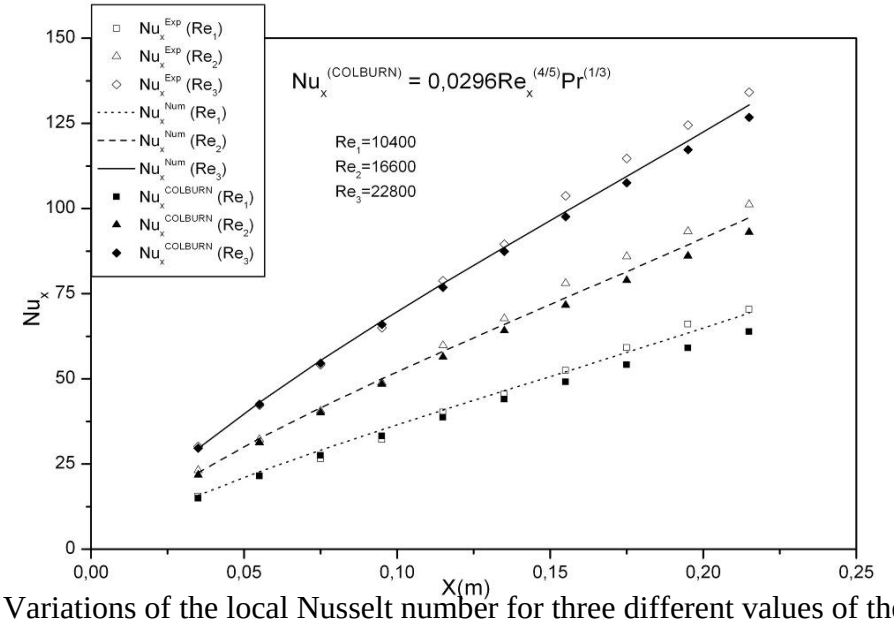

Figure 9. Variations of the local Nusselt number for three different values of the Reynolds numbers: Re_1=10400, Re_2=16600, and Re_3=22800.

Part 2: Increase in heat transfer in the presence of an obstacle The next experiments were concerned with the evolution of the total heat flux density in the presence of an obstacle (37 cm wide x 2 cm high x 2 cm thick) placed transversely (aligned with the Z-axis) on the lower isothermal plate (Figure 1). The purpose of this series of measurements is to quantify the heat transfer increase due to the presence of an obstacle. However, the paper does not discuss the effect

of the obstacle's geometry (cross section) on the heat transfer rates to avoids making it overly lengthy.

Solution independence with grid refinement (both angular and directional) was verified. The number of control volumes used in this section is 141054 while an S4 angular discretization was used. Numerical simulation involving the *k*-ε model were obtained and the results are presented in figures 10 and 11 along with corresponding experimental results.

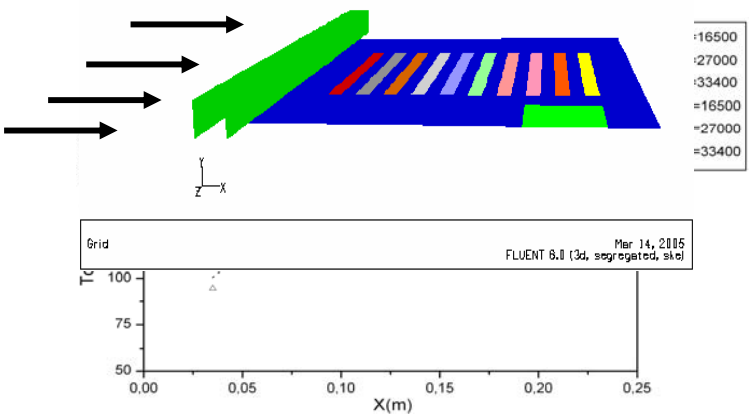

Figure 10. Total heat flux in the flow direction for different Reynolds numbers behind the solid body Re=16500 (dotted line), Re=27000 (dashed line) et Re=33400 (solid line), symbols represent experimental values. Air temperature is T_0 =296 K and temperature, cold isothermal plate T_1=287.7K and hot resistance temperature T_2=301.1K.

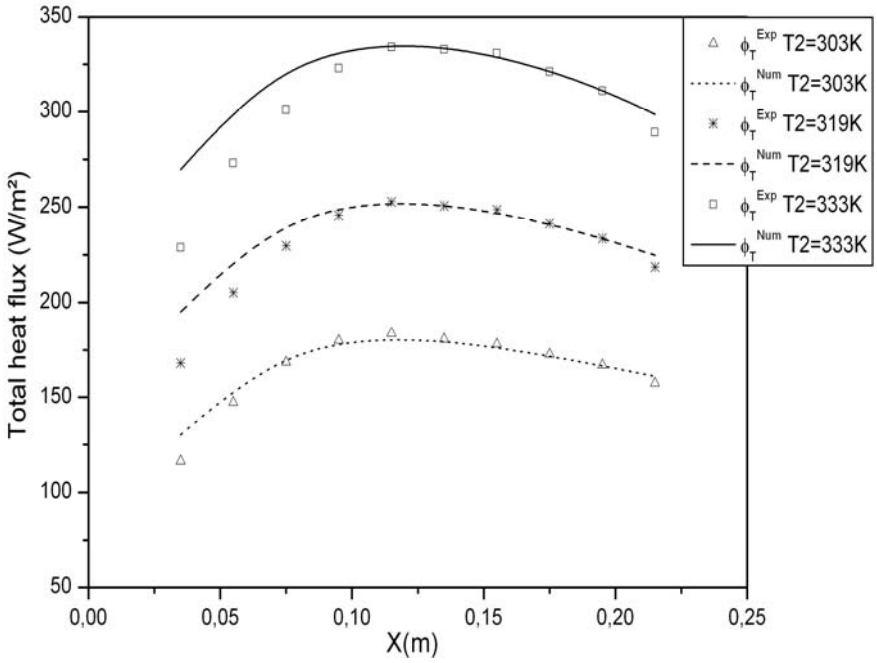

Figure 11. Total heat flux in the flow direction for different gradient temperature behind the solid body ΔT=12 K (dotted line), ΔT=28 K (dashed line) et ΔT=42 K (solid line). Reynolds number is Re=24100, symbols represent experimental values. Air temperature is T_0 =296 K.

The separation zone, in the immediate vicinity of the obstacle, is an area of minimum heat transfer, while the reattachment zone, located further downstream, constitutes a more important heat transfer area. Heat transfer is expected to increase in the region where the viscous sublayer develops. Figure 10 clearly reflects the above-discussed physics. The obstacle's wake is shown to cause a turbulent motion in the flow, thus improving overall convective heat transfer. Therefore, this work is of interest for the study of heat transfer and opens a perspective for the development of our present study.

Figure 11 presents an increase in heat transfer versus temperature. After the fifth fluxmeter, the exchanged heat takes its maximal value, and then decreases until the exit of the channel's plate. The relative variation between numerical and experimental results is less than 6%. Figure 11 emphasises the influence of the radiation in this area. When the resistance's temperature increases, a gap is created in the separation zone between experimental and numerical results with a maximum of 13%.

In the ultimate experiment presented here, the location of the obstacle is modified in order to highlight the flow recirculation effects on heat transfer. The width of the obstacle is decreased to 1cm so as to fit it between the fourth and the fifth fluxmeter (at X = 0.08 m). As in the previous experiments, the test zone is submitted to forced convection as well as radiation. Experimental and numerical results are plotted in figure 12. There is an important change in thermal exchanges upstream of the obstacle (maximal value right at the fourth fluxmeter). A large and abrupt decrease of the overall heat flux is shown as soon as the flow passes over the edge of the obstacle. The thermal flux then rises until the exit of the plate, location of the second recirculating zone with negative velocities.

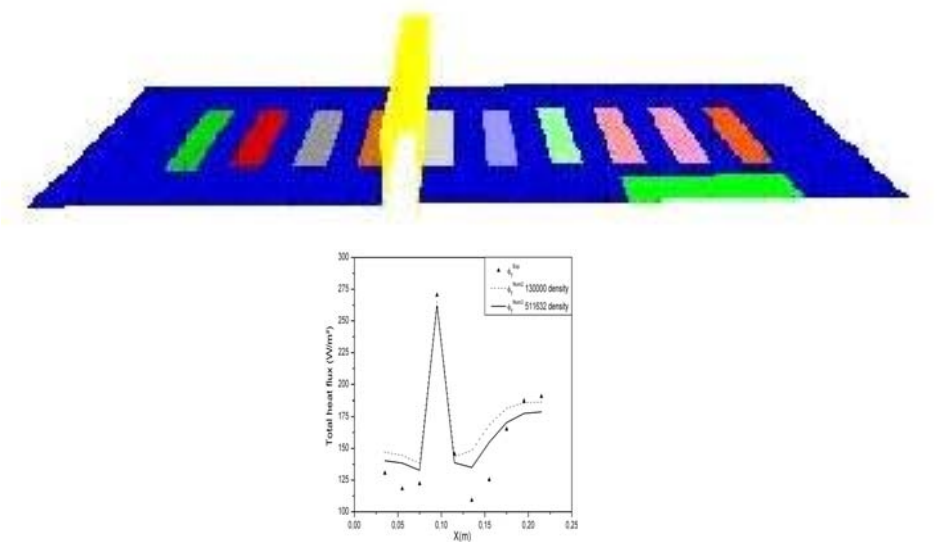

Figure 12. Total heat flux density in the flow direction behind the solid body located between the fourth and the fifth heat flux sensor. Cold isothermal plate T_1=287.7K, hot resistance temperature T_2=303.1K and air temperature T_0=296K. Reynolds number is Re=9670, symbol represents experimental values. Two different meshes are used, dotted line is for 130000 control volumes and the solid line is for 511632 control volumes.

The numerical and experimental results show a similar evolution, Nevertheles, one can notice a significant difference between the values predicted and those that were measured. The maximum discrepancies occur near the sixth fluxmeter. This is due to the interaction between negative velocities of some fluid particles which come back to the obstacle, and positive velocities of the turbulent fluid in this area. The highest relative difference found is 18%. Insufficient grid refinement was suspected here and the results are shown for two different grid refinements. Unfortyunately, we were not able to refine the grid further as the capacity of our machines were pushed to their limits. This should now be investigated more thoroughly.

CONCLUSION

In this paper, a numerical investigation of turbulent forced convective flow in a horizontal channel with rectangular obstacles located on the lower wall is carried out Various turbulence models were tested and results were compared with experimental data. The turbulence model which was retained here is the k-ε one. In all cases, the resolution scheme is stationary. It is noted that the relative error between the numerical and experimental results, never exceeds 5% except in th case of the obstacle. The last experiment is related to the evolution of the total heat flux in the presence of an obstacle of size (37cm, 2cm, 2cm) placed transversely upstream of a horizontal and isothermal plane plate.
The objective of this disposition was to quantify the increase in the heat transfer due to the obstacle. Passing through the obstacle, the flow separates. The zones of separation are synonymous of minimum heat transfer, while the sticking zones constitute zones with very good transfers. This is due to an important friction at the wall related to this sticking.
The heat transfer continues to increase in the area of development of the viscous sub layer.
The wake after the obstacle causes a swirling movement in the fluid, thus improving the convective heat transfers. The grid used in this part is tightened around the obstacle for the best taken more into account of the dynamic phenomena in the flow. This work is interesting with regard to the increase in heat transfer. Numerical results and experimental data obtained with heat flux sensors are very useful in this way. The influence of the obstacle geometry was not studied but could be the subject of future studies.

REFERENCES

ASTM Building Applications of Heat Flux Transducers, [1985], *ASTM* STP 885, Ed Bales, Bomberg, Courville.

Bejan, A., [1995], *Convection Heat Transfer*, 2nd ed. Wiley.

Burmeister, L.C., [1993], *Convective Heat Transfer*, 2nd ed. Wiley.

Degenne, M., Klarsfeld S., [1985], *Building Applications of heat Flux Transducers*, ASTM STP 885, E BALES, M. BOMBERG AND G.E. COURVILLE, Ed. American Society for Testing and Material, Philadelphia, 163-171.

Fluent 6.2 Documentation, *Fluent Inc*, [2003].

Holman, J.P., [2002], *Heat Transfer*, 9th ed., McGraw-Hill.

Incropera, F.P., Dewitt, D.P., Bergman, T., Lavine, A. [2006], *Fundamentals of Heat and Mass Transfer* 6th ed., Wiley.

Kobus C.J., [2005], Utilizing disk thermistor to indirectly measure convective heat transfer coefficients for forced, natural and combined (mixed) convection, *Int Rev. Experimental Thermal and fluid Science*, 29, 659-669.

Launder B.E., and Spalding D.B., [1974], The numerical computations of turbulent flows, *Computer methods in applied mechanics and engineering*, 3, 269-289.

Lassue S., [1989], Analyse des échanges radiatifs et convectifs à la surface d'une paroi opaque. Application à la commande optimale du système habitat. Thèse de doctorat de l'université de Lille 1.

Leclercq, D., Thery, P., [1983], Apparatus for simultaneous temperature and heat flux measurements
Under transient conditions, *Rev. Sci. Instrum*, 54.

Lefevre, J., [1986], *Mesure des debits et des vitesses des fluides*, Ed Masson.

Patankar, S.V, [1980], *Numerical Heat Transfer and Fluid Flo*w, Hemisphere, N.Y.

Sternfield, H.J. and Reinkenhoff, J., [1977], Technics for determining local heat transfer coefficient, *AIAA Journal*, 15, 1.

Tsirel'man N.M., [1973], Determination of the heat transfer coefficient from the law of constant-temperature front propagation, *J. Eng. Phys*., 25, 2.

Wong H.Y., [1979], The measurement of convective heat loss from a solid surface to an airstream, *J. Phys. E. Sci. Instrum.*, 12.